Effect of Field Cooling on Magnetic Domain Memory in Exchange Coupled Thin Films

Matthew Rytting

A senior thesis submitted to the faculty of
Brigham Young University
in partial fulfillment of the requirements for the degree of

Bachelor of Science

Karine Chesnel, Advisor

Department of Physics and Astronomy

Brigham Young University

August 2012

ABSTRACT

Effect of Field Cooling on Magnetic Domain Memory in Exchange Coupled Thin Films

Matthew Rytting
Department of Physics and Astronomy
Bachelor of Science

It has been found that magnetic domain memory can be induced in ferromagnetic thin films via exchange coupling with a antiferromagnetic layer. This effect was first observed in a zero field cooling state (that is, after cooling the material below the blocking temperature in the absence of an external magnetic field). In this project, we explored the effect on magnetic domain memory when the sample is field cooled (cooled in the presence of an external field). Our sample consists of multilayers of [Co/Pd] paired with an antiferromagnetic IrMn alloy. This combination exhibits exchange coupling. We used X-ray Resonant Magnetic Scattering to study the domain morphology. We analyzed the data using a cross-correlation technique. The results of our study show that the material gradually loses memory when the sample has undergone field cooling as well as that the region of highest memory is shifted due to exchange bias.

Keywords: magnetic domain memory, exchange bias, x-ray scattering, cross-correlation

ACKNOWLEDGMENTS

I would first like to thank the College of Physical and Mathematical Sciences, and the Physics and Astronomy Department in particular, for giving me the opportunity and the funding to do this research. I am especially grateful to Dr. Karine Chesnel for allowing me to join her group. She has been very patient as I learned about this subject. She has given me great opportunities to do research in world class facilities and helped me throughout this project. Also, I would like to thank Dr. Van Huele and Dr. Ware for teaching me how to write this thesis. Most importantly, I would like to thank my wonderful wife, Stephanie, for supporting me through the times when I was spending long hours away doing this. She is amazing.

Contents

List of Figures

Chapter 1

Introduction

1.1 Motivation

Data storage is cheaper than ever before, yet the demand continues to grow. Beyond the need for storage for data for companies, government, and personal use, there is currently a proliferation of hand-held devices which require denser memory storage. These demands have led to the investigation of the properties of thin magnetic films. In such films, when the thickness of magnetic layers is finely adjusted, the magnetization tends to prefer perpendicular orientation rather than in-plane. [1] Perpendicular thin films exhibit ferromagnetic domains, i.e. regions where magnetic moments are aligned as explained in Section 1.3. The size of these domains is a crucial parameter for the potential storage density of the material, and make thin films attractive objects of study.

Most common magnetic storage devices currently have two main limitations. First, they are limited in their spatial memory density. As technological devices become increasingly compact, the limiting factor is quickly becoming data storage density, particularly in magnetic-based data storage. [2] The second limitation is the susceptibility to modification or erasure by external magnetic fields. Stray magnetic fields eventually corrupt magnetic data storage devices, so long-term

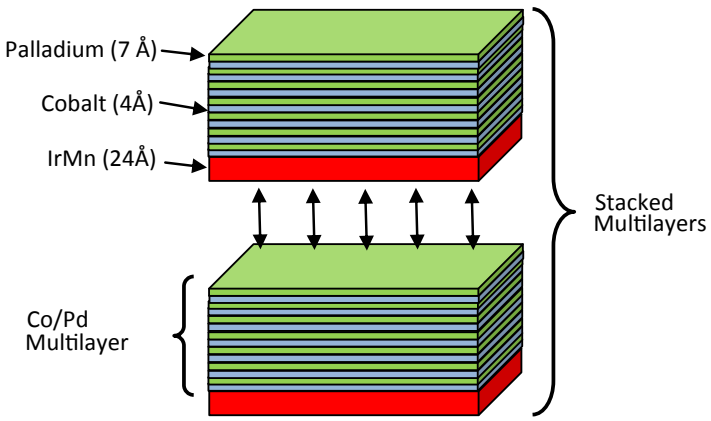

Figure 1.1 Our sample contains of a $[Co/Pd]_{12}$ multilayer combined with an IrMn layer. Four sets of these groupings are stacked together.

archives must be rewritten periodically (typically every four years). Our research is focused on a more fundamental understanding of magnetic thin films. We are studying ways to force ferromagnetic systems to return to a set domain morphology, even after they have been saturated. This reproducibility of specific domain morphology is what we call magnetic domain memory (MDM). We propose to study the reversal and MDM properties in such films when they have been field cooled.

1.2 The Sample

Our sample consists of both ferromagnetic and antiferromagnetic materials. The primary component is thin layers of cobalt four angstroms thick. This thickness was optimized to force the spins to point into or out of the plane of the sample rather than in plane. [1] These Co layers are paired with seven angstrom thick layers of palladium so as to make a multilayer. There are then 12 Co/Pd pairs stacked together; this [Co/Pd] multilayer makes up our ferromagnetic material. An antiferromagnetic layer of an IrMn alloy is then inserted which is 24 angstroms thick. This combination of [Co/Pd] multilayers and IrMn is repeated four times. This can be seen in Fig. 1.1.

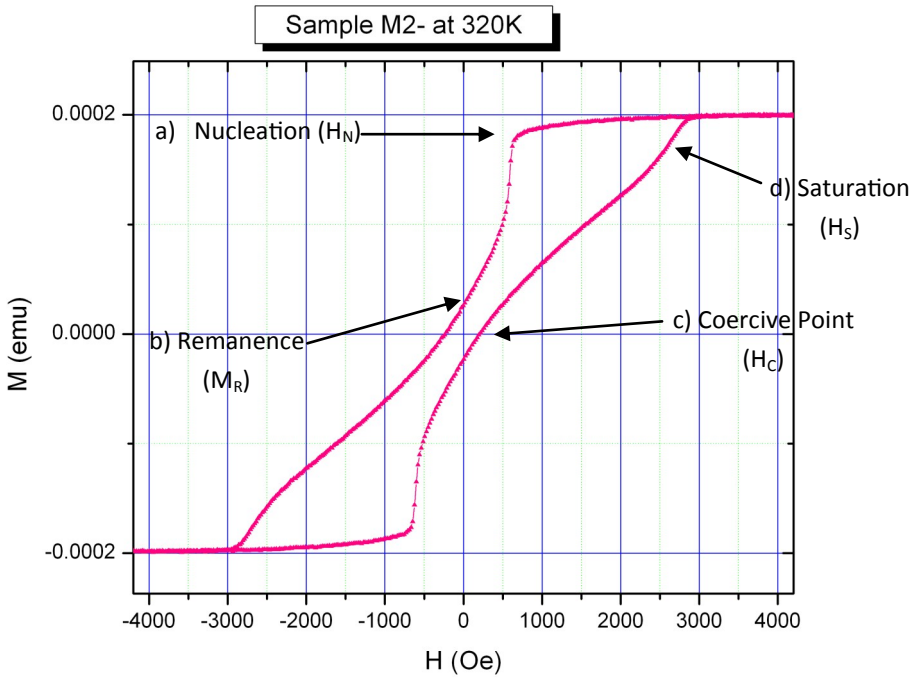

Figure 1.2 A sample hysteresis loop. Note that the ascending and descending branches,while symmetrical, do not match. Points of interest: a) Nucleation is where the domains begin to rapidly change from saturation to match the applied field. b) Remanence is the remaining net magnetization when the applied field is zero. c) The coercive point is when the net magnetization of the sample is zero. d) Saturation is when essentially all of the domains are aligned to the applied field.

1.3 Ferromagnetism and Hysteresis

One specificity of ferromagnetic materials is the formation of domains. These domains are characterized by the constituent atomic spins all pointing in the same direction; in the absence of other magnetic fields, the domains are generally oriented randomly. However, when an external field is applied, the domains align to the applied field (and merge together to form larger domains). With a strong enough field, all of the domains in the sample essentially become one large domain with all the spins aligned to the applied field. This condition is what we call saturation (H_S).

Another characteristic of ferromagnetic materials is the possible occurrence of hysteresis. As

one applies a varying field to the sample, the net magnetization of the sample changes as the domains align to the field. The field is often applied in a loop. First one would sweep the field in the increasing direction (the ascending branch), and then sweep the field in the decreasing direction (the descending branch). In samples like ours, the ascending and descending branches of the magnetization loop do not match. This is hysteresis; the net magnetization of the sample is path dependent, as is illustrated in Fig. 1.2. Although the net magnetization of the sample is different for the ascending and descending branches, the hysteresis loop is usually fairly symmetrical. For the same applied field, such as H = 0, the net magnetization of the sample on the descending and ascending branches is opposite in value. This remaining magnetization when there is no applied field is refereed to as remanence (M_R). Other field values of importance are H_N, the value at which domains begin to nucleate when cycling the field away from saturation, and H_C, the field at which the net magnetization is zero.

1.4 Magnetic Domain Memory

One may also note that in a given loop there are usually two points with the same net magnetization. While the net magnetization is the same, the shape of individual up and down domains, or the local morphology, may be different. An example of domain morphology of our sample is shown in Fig. 1.3. This image was taken at room temperature with no applied field. It is 10 μm square, and the up and down domains are visualized by the light and dark stripes. Here the domains are, on average, approximately 200 nm wide. MDM is the ability for the domains to retrieve their same local configuration after an applied field loop. It has been previously shown that ferromagnetic material can exhibit high MDM through the use of defects. [3] This was usually in the nucleation stage. Here, we induce MDM via another route - not defects, but through exchange coupling.

1.5 Exchange Coupling

Unlike with ferromagnetism, antiferromagnetic domains have anti-parallel spins as shown in Fig. 1.4. Thus, in the bulk of the antiferromagnetic material, the net magnetization is zero. When there is an interface with a ferromagnetic layer, the spins tend to align in parallel through a process called exchange coupling. This causes some net magnetization, and these spins are referred to as uncompensated spins. Thus the ferromagnetic layer imprints its domain morphology onto the antiferromagnetic layer.

The uncompensated spins in the IrMn still respond and align to the changing ferromagnetic domains above what is called the blocking temperature (approximately 300 K for this sample). When the sample is brought below its blocking temperature, the spins lock and no longer respond to the changes caused by an external field to the ferromagnetic domains. The locking of spins gets stronger at lower temperatures. Exchange coupling serves as a medium for creating materials with high MDM.

The cooling of the sample below the blocking temperature can be done either with or without

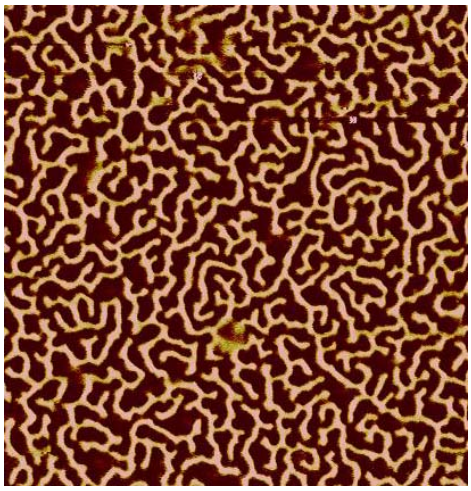

Figure 1.3 An image taken via magnetic force microscopy (MFM) of our sample with no applied field at room temperature. Here the up and down domains are visualized as the light and dark lines. This is a 10 μm square image.

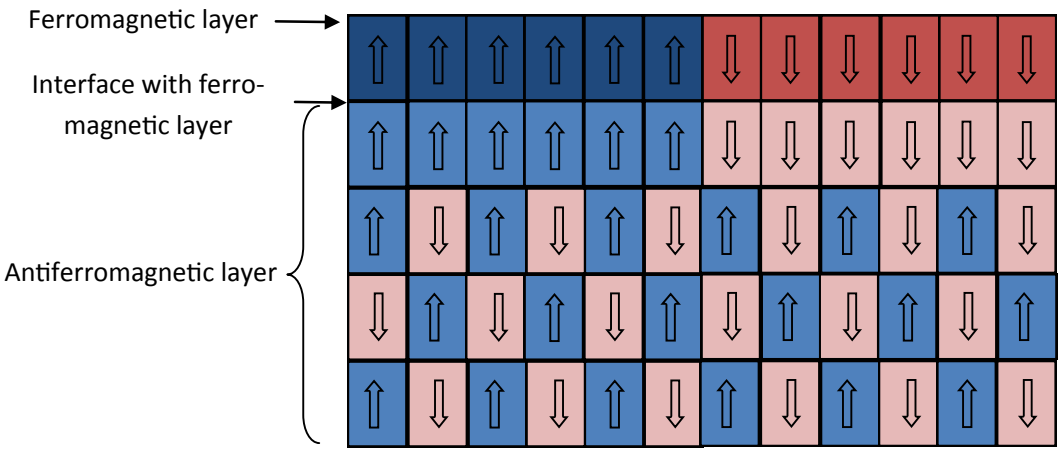

Figure 1.4 An example of atomic spins antiferromagnetic material. In the bulk the spins are aligned anti-parallel (represented by the up and down arrows) and there is zero net magnetization. At the boundary, however, there are uncompensated spins which form domains more similar to ferromagnetic material.

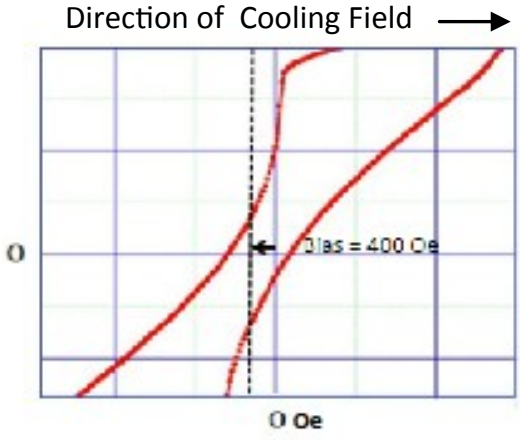

Figure 1.5 This is a zoomed in image of Fig. 1.2 showing the bias introduced from the Field Cooling. The applied field during cooling as applied toward the right of the graph causing the bias to the left.

an external magnetic field. When an external field is present during cooling, this process is called field cooling (FC). Zero Field Cooling (ZFC) is done in the absence of an external field. The effect of FC is to introduce a bias to the hysteresis loop. This exchange bias is an effect of exchange coupling in field cooling. This effect is clearly seen in Fig. 1.5. The field we applied toward the right (positive direction) of the graph causes a bias to the left (negative direction) (in Fig. 1.5). The bias is in the opposite direction of the cooling field because the uncompensated spins of the antiferromagnetic layers are locked with a majority of them in the direction of cooling field. This causes a net magnetization in the positive direction. Thus, it takes a greater external field in the opposite direction to counterbalance and reach no net magnetization.

1.6 Previous work

Our study of this material began with quantifying the degree of MDM when it was under ZFC conditions. Two former students, Brian Wilcken and Joseph Nelson helped develop some of the analysis tools used for my study, and applied them to the ZFC case. It was shown that exchange coupling was effective at creating high MDM. [4]

Brian Wilcken focused on creating interfield maps of the MDM in the ZFC state. Interfield maps show the amount of memory when images are compared between applied field (H_1) in one loop and the applied field (H_2) in another loop. This creates a two dimensional map of the memory. In order to do this, Brian developed a Matlab code to determine the degree of correlation between images. His program isolates the parts of the image which are necessary for determining the degree of MDM, compares the images, and outputs maps of the various memory values. [5] The program will be explained in more detail in Sec. 2.2 and 2.3. Joseph focused on q-selective memory where q stands for a given radius of the pattern in the images. [6] These images and how they were obtained will be explained further in Section 2.2.

1.7 Goals

For my study, I have used two techniques: Magnetic Force Microscopy (MFM) and X-Ray Resonant Magnetic Scattering (XRMS). These are complimentary tools. MFM allows us to get a visualization of the physical domain pattern in real space, while XRMS gives a visualization of the domains in scattering space. We have primarily used the data collected via XRMS to quantify the degree of MDM. We have done this by cross-correlating the images (see Ch. 2). We generated interfield maps using the field cooling data. Through this process, we determined the effect of field cooling on memory and have shown that it actually lowers the degree of memory relative to ZFC, although there is still significant MDM (see Ch. 3).

Chapter 2

Imaging Techniques

2.1 Magnetic Force Microscopy

Magnetic Force Microscopy (MFM) is a scanning microscopy technique to visualize the domain pattern in magnetic materials. MFM is an imaging technique closely related to Atomic Force Microscopy (AFM). In AFM, a small tip only a few nanometers across at its point is oscillated at high frequency (around 100 kHz) near the surface of the sample. A laser is reflected off the tip, and when the tip interacts with the atoms of the sample, the deflection of the laser is measured and used to create a visual image of the height and width of the sample's surface features. The tip scans the surface horizontally before moving a few nanometers over and traversing the sample again. These one-dimensional passes are combined to create a two dimensional image. MFM uses a cobalt coated tip so that magnetic interactions can also be measured. As shown in Fig. 2.1, after an AFM pass is conducted the tip raised to a lift height of typically 20 - 50 nm and follows the physical topography previously recorded exactly so that the only deflections of the tip come from magnetic forces.

MFM is not a tool for measuring magnetic memory because it is difficult to compare the images

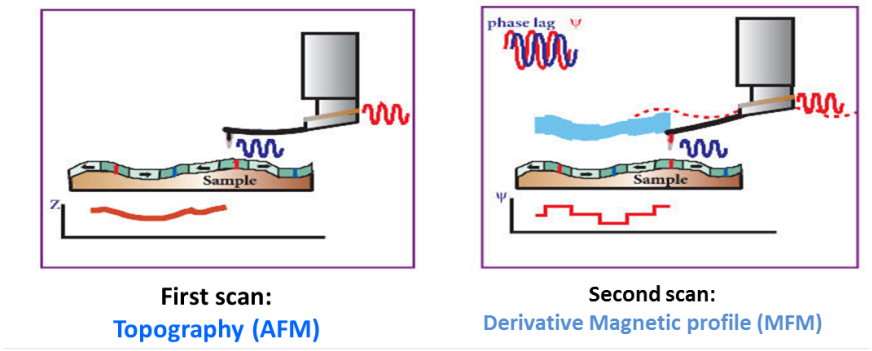

Figure 2.1 This is a diagram of the MFM process showing the lifting of tip to eliminate the effect of the physical features to leave only the magnetic forces.

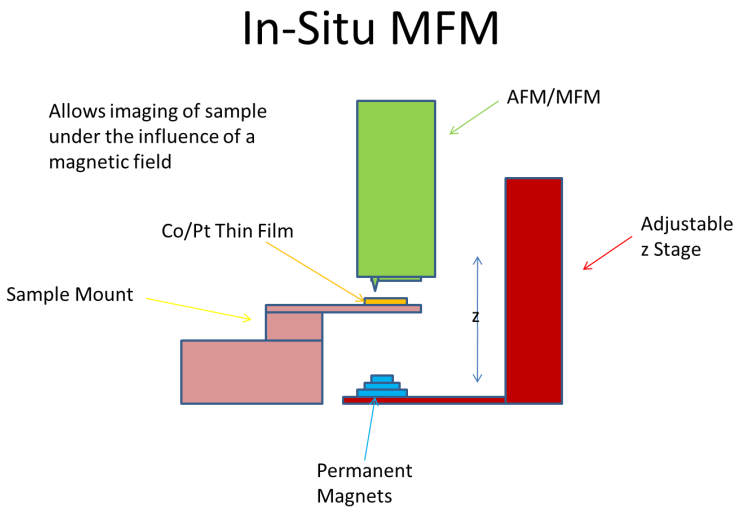

Figure 2.2 This is a diagram of our *in-situ* MFM set-up

easily for similarity since the sample tends to move over the course of several images. Additionally, the strong magnetic domain memory (MDM) caused by exchange coupling only occurs at low temperature and we can only perform MFM at room temperature with our instrument. However, MFM is great for visualizing domain patterns in real space. I began with this tool to visualize how the sample looked and behaved physically (for the structure of the sample refer back to Fig. 1.1). Extra *in-situ* magnetic imaging capability was added with the help of to another member of our group, Andrew Westover. In this setup, a set of permanent magnets are placed on a translational

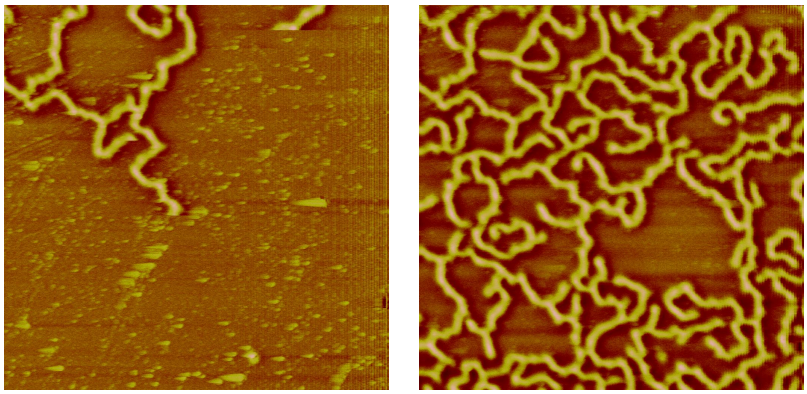

(a) $H = 548Oe$ (b) $H = 348Oe$

(c) $H = 262Oe$ (d) $H = 18Oe$

Figure 2.3 The series of MFM images shows the progression of the sample's domains as the field goes from saturation toward zero. Image (a) shows the beginning nucleation with just a few domains. Images (b) - (d) show the growth of the original domains. Not that you can see the opening structure throughout.

stage so that they can be raised and lowered beneath the sample as illustrated in Fig. 2.2. This allowed us to control the field applied *in-situ* and to see how the domain pattern changes with applied field throughout a magnetization loop. A selection of 10 μm images taken at room temperature on a descending branch (from nucleation to remanence) are included in Fig 2.3.

2.2 X-Ray Resonant Magnetic Scattering

X-Ray Resonant Magnetic Scattering (XRMS) is a technique developed in the 1980s which uses X-rays generated by synchrotron radiation to study magnetic domain morphology. [7–9] The energy of the X-rays is tuned to a resonance edge of the magnetic material in the sample. For an L_3 transition, the energy is set to excite electrons from the (2p) to the (3d) orbitals. After causing this excitation, the photons are scattered. In our case, the resonant edge was the L_3 edge of Cobalt, at about 780eV. [10] These scattered photons are captured by a CCD camera to create a 2-D image. In order to tune the energy to specific edges and the necessary coherence for our analysis, these experiments can only be performed at a synchrotron facility. The set of data I worked on was done at the ALS at Lawrence Berkeley National Lab. We also took further data at the APS at Argonne National Lab.

During the experiment, X-rays are scattered through our sample, as shown in Fig. 2.4. The light which is transmitted is stopped by a blocker. The scattered X-rays create an image on the CCD camera (see Fig. 2.4). The shape here is a ring where the radius corresponds to the periodicity of the magnetic domains. The ring shape comes from the fact that there is no preferred orientation for the domain stripes, but instead the morphology is a "maze", with isotropic domains like in Fig. 1.3.

The XRMS images we obtain are a transform of the physical features into scattering space. Fig. 2.5 illustrates the geometry of the scattering. Here the scattering vector, q, is defined by the

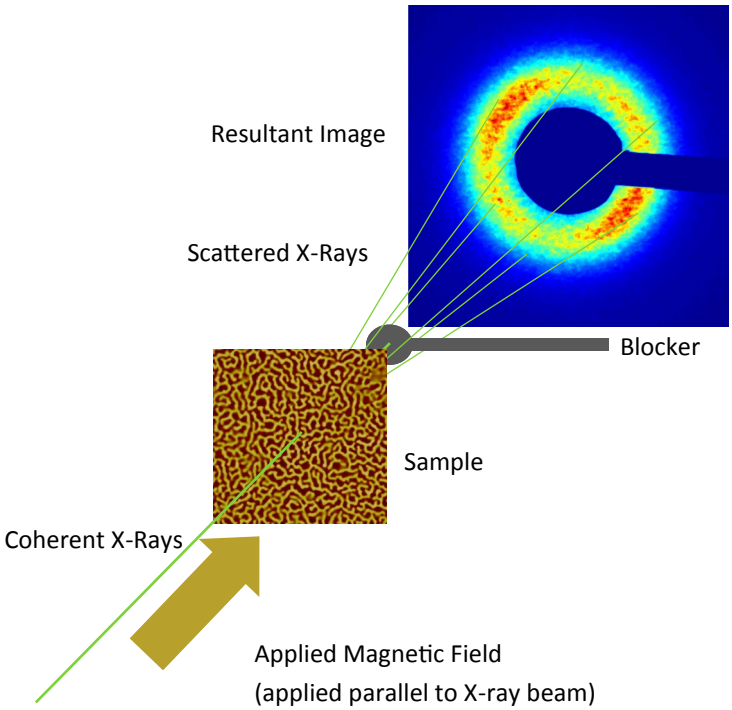

Figure 2.4 A diagram of the experiment at the synchrotron showing how the light enters the sample and is captured. The X-rays transmit through the sample and are scattered. The scattered photons are captured by a CCD camera. [11]

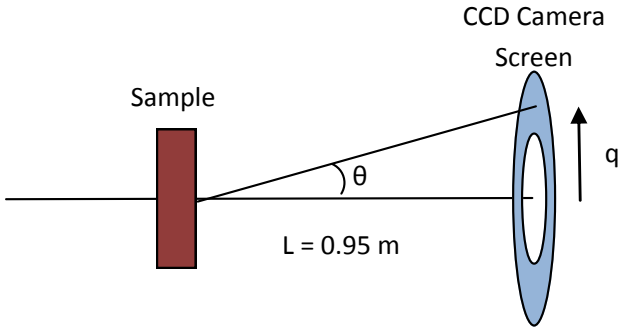

Figure 2.5 This is a sketch of the scattering geometry in our experiment. The signal is collected for a range of q values.

relationship

$$q = (2\pi/\lambda)\sin\theta \tag{2.1}$$

where λ is the wavelength of the incoming coherent X-rays and θ is the scattered angle. The scattered light is most intense when q matches a Bragg peak in the reciprocal space relatinoship:

$$q = 2\pi/d \tag{2.2}$$

where d is the size of the structural features. In our sample, d corresponds to the period of the domains. By combining Eq. 2.1 and Eq. 2.2 one arrives at the familiar transmission geometry version of Bragg's law:

$$d\sin\theta = \lambda. \tag{2.3}$$

The angle is scanned, and the angle at which the most intense scattering occurs can be calculated knowing the distance between the sample and the camera (L = 0.95 m) and the radius of the image. With a wavelength of $\lambda = 1.59$ nm, the periodicity of the domains is found to be about $d = 400$ nm; this agrees with the measurements of period obtained using MFM.

These images generally contain both magnetic and charge scattering. The charge scattering comes from all structural features of the sample while the magnetic scattering comes from all of the magnetic features. Our sample is a smooth film, and the charge scattering is very small. It also appears at lower q than the magnetic scattering. The charge scattering is not beneficial in a study of memory, because one would expect the overall structure of the sample to remain unchanged while cycling the field. If it were included, it would artificially increase the degree of similarity between images.

Fig. 2.6 shows a series of images taken along one branch of a field cycle. The first image, taken near nucleation, displays a disk shape. The second image transitions to, and the third image

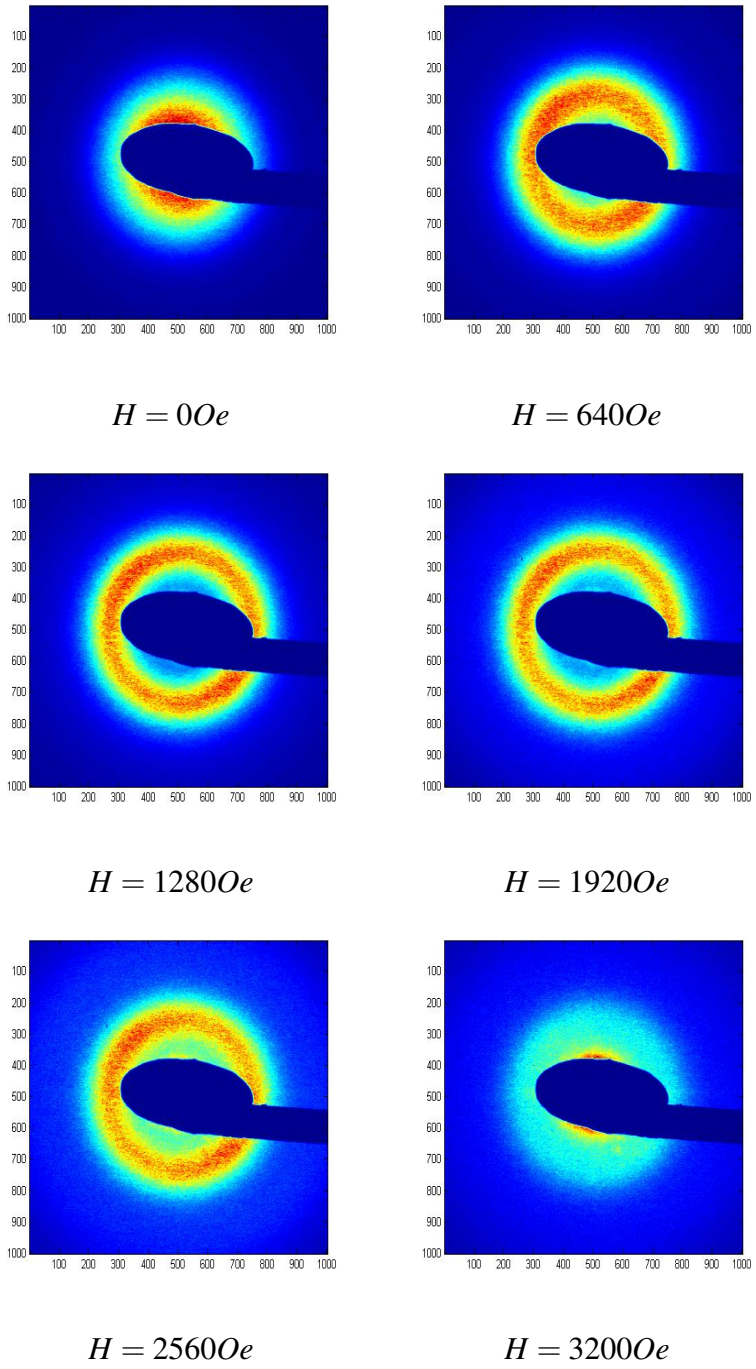

Figure 2.6 A series of XRMS image showing the strong ring feature of the scattering as it changes in size due to applied field. Red indicates high intensity while blue is low. The shape in the middle is caused by a blocker which catches the unscattered X-rays.

attains, a ring state indicating that the sample is near zero net magnetization. The fourth and fifth images show the ring weakening until, by the last image, the ring dissipates as the sample reaches saturation.

There are additionally two types of magnetic scattering: coherent and incoherent. In the images shown in Fig. 2.6, the strong ring is mostly made up of incoherent scattering with the coherent scattering on top of that "envelope". The images were processed to isolate the coherent magnetic scattering which gives us the true "shape" of the magnetic structure of the sample. The images were smoothed to approximate the incoherent magnetic scattering envelope in the image and then by subtracting the envelope from the raw images we extracted the magnetic "speckle". Fig 2.7 shows the speckle of a processed image as the small red and yellow spots. The process of obtaining the incoherent envelope and subtracting it from the raw image is visualized in Fig. 2.8. This process required finding the right balance of smoothing enough to get a good envelope and avoid subtracting out any speckle, but not smoothing so much as to under average and leave some of the envelope. The incoherent scattering is related to the average domain period of the sample and is fairly consistent when cycling the field. The coherent speckle, however, gives us a unique "fingerprint" of the specific domain morphology of the sample. Thus it is crucial to isolate the speckle in order to do a true study of the degree of correlation between our images. Leaving in the incoherent envelope would artificially inflate that degree of correlation.

2.3 Cross-Correlation Technique

We used a cross-correlation technique to quantify the amount of similarity between images. To speed the cross-correlation, the images undergo a Fourier transform and are then multiplied before undergoing an Inverse Fourier transform to determine the degree of similarity between the images. The resulting correlation pattern image presents a peak as its center such as in Fig. 2.9. The peak's

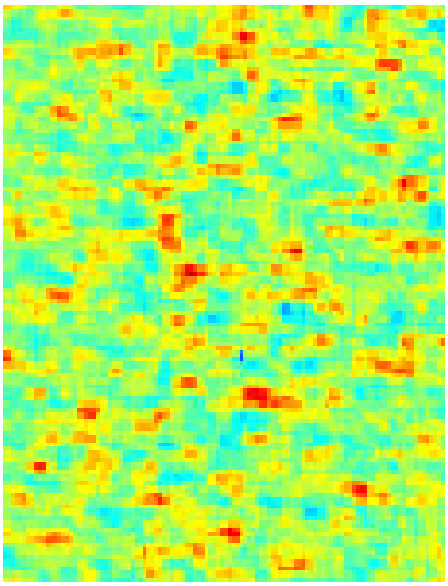

Figure 2.7 An image of the isolated speckle. This is zoomed in from a processed image so that the speckle is more visible. This image is approximately 100 by 200 pixels.

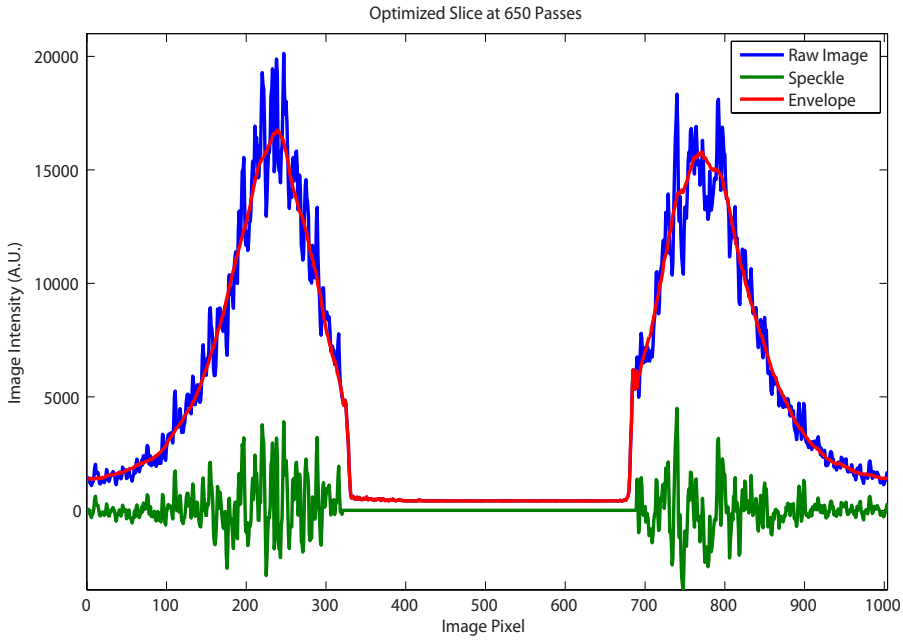

Figure 2.8 Slices through a raw scattering image (such as in Fig. 2.6), the smoothed envelope, and the remain speckle. These slices are taken vertically in the middle of the image. The area of zero intensity is where the slice crosses the blocker. By subtracting the smoothed curve from the raw data, the speckle is what remains.

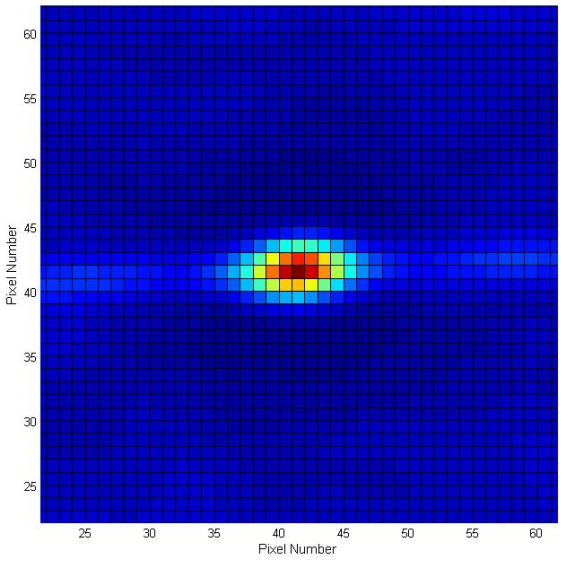

Figure 2.9 The process of comparing two images pixel by pixel constitutes the cross-correlation process. The result of which gives us a large central peak as shown. Note that the peak image is zoomed in around the peak since the peak is so small compared to the total image.

average size is typically about 5 by 10 pixels and this actually corresponds to the average size of each speckle. The fact that we get such an intense peak shows that there is a great amount of similarity between the given images. If there is little similarity, the correlation peak is weak and not easily visible. Thus, the size of the peak tells us how similar the domain morphology is between the two points of measurement and, consequently, the amount of MDM.

To quantify the amount of MDM, we integrate the peak and normalize by the autocorrelation. Since the only region of interest is right around the peak, we integrate only a selected ellipse which surrounds the peak. This integrated value is normalized by dividing it by the correlation values of the images making it up. For instance, if comparing images A and B, then $A \times B$ is divided by the

	$b=1$	$b=2$	$b=3$	$b=4$	$b=5$
$a=3$	0.615	0.626	0.627	0.627	0..628
$a=4$	0.632	0.635	0.637	0.639	0.639
$a=5$	0.640	0.642	0.645	0.645	0.646
$a=6$	0.648	0.650	0.651	0.651	0.651
$a=7$	0.652	0.653	0.655	0.655	0.655

Table 2.1 Values of rho for a correlation between a pair of images with given ellipse parameters as we sought to optimize the integration area. Here a stands for the semi-major axes and b for the semi-minor axis of the ellipse. We found that the larger the integration size the better value for ρ. This leads us to believe the program was doing something different than we thought it was since we would expect to find an optimum ellipse size.

square root of $A \times A$ and $B \times B$ to normalize and obtain a value between 0 and 1. This value is called ρ and is indicative of the degree of MDM.

$$\rho = \frac{A \times B}{\sqrt{(A \times A)(B \times B)}} \tag{2.4}$$

The peak was integrated by choosing an ellipse around the peak and integrating those points within the ellipse. The size of the ellipse has an effect on ρ. Table 2.1 shows a systematic study I conducted on this effect. We found that there was no optimal size at which ρ was biggest and then smaller at all others. Instead, the larger the integration ellipse, the larger the value of ρ. This led us to conclude that we should simply choose an ellipse that just encompasses the peak. To make it any larger would artificially inflate the value of ρ calculated.

Chapter 3

Results and Discussion

3.1 Return and Conjugate Point Memory

My research project was to determine the effect of applying an external magnetic field during cooling on magnetic domain memory (MDM). A first approach was to characterize the memory only at the return point and the conjugate point of the hysteresis loop. The return point is obtained when the applied field is the same between two branches (so it would compare points on an ascending branch of one loop with the ascending branch of successive loops). The conjugate point is obtained when the applied field is exactly opposite, and would thus compare an point on an ascending branch with a point on a descending branch. The calculated MDM at these points are referred to as Return Point Memory (RPM) and Conjugate Point Memory (CPM). There are some distinctive characteristics of the curves in Fig. 3.1-3.7. One interesting feature is the low degree of memory at nucleation and saturation. Nucleation and saturation follow a similar process where the sample is in a state of transition toward or away from a single domain state. The fact that the memory is so low at nucleation implies that domain nucleation is quite random. We observe that CPM is generally slightly lower than RPM in Fig. 3.1-3.7. The reason for this difference is the bias

introduced by FC. The bias causes the conjugate points to not fully line up. Even in a ZFC state we found that the CPM was slightly lower than the RPM, but here, bias leads to a greater difference between the two points. Further, it is interesting to note that the memory decreases, both in RPM and CPM as the field applied during FC (H_{FC}) is increased.

Figures 3.1-3.7 show another interesting trend. While in the ZFC state the memory was quite stable over several field cycles, in FC the memory decreases significantly with greater separation between cycles. This decrease is fairly consistent throughout the cycles, and results in a decrease in ρ of approximately 0.1 with each increase in loop separation. ρ lost by increasing loop separation does increase with greater H_{FC}. It is actually quite interesting that this decrease is so consistent despite the fact that the maximum MDM values are different between the different series. That does mean, however, that the percentage of The exception to this rule is the $H_{FC} = 3200$ Oe series. Here the MDM is once again quite stable. The $H_{FC} = 3200$ Oe series has more loops than the other series, and it shows that the decrease in MDM from increased loop separation slows down. Unfortunately, this is the only series with so many loops so we cannot be sure that this trend always occurs.

3.2 Interfield Maps of Magnetic Domain Memory

Our next step consisted of creating two-dimensional maps of ρ. This analysis is more complete than the one-dimensional graphs and consists of calculating not only RPM and CPM values, but calculating the memory between all pairs of fields within the hysteresis loop. The applied field during the loop is referred to as H, thus these $H_1 \times H_2$ interfield maps consist of values of ρ at every field combination.

A prominent feature on all the maps is that the highest memory is along the axis of the return points where $H_1 = H_2$, which corresponds to RPM. We learn from interfield maps that MDM

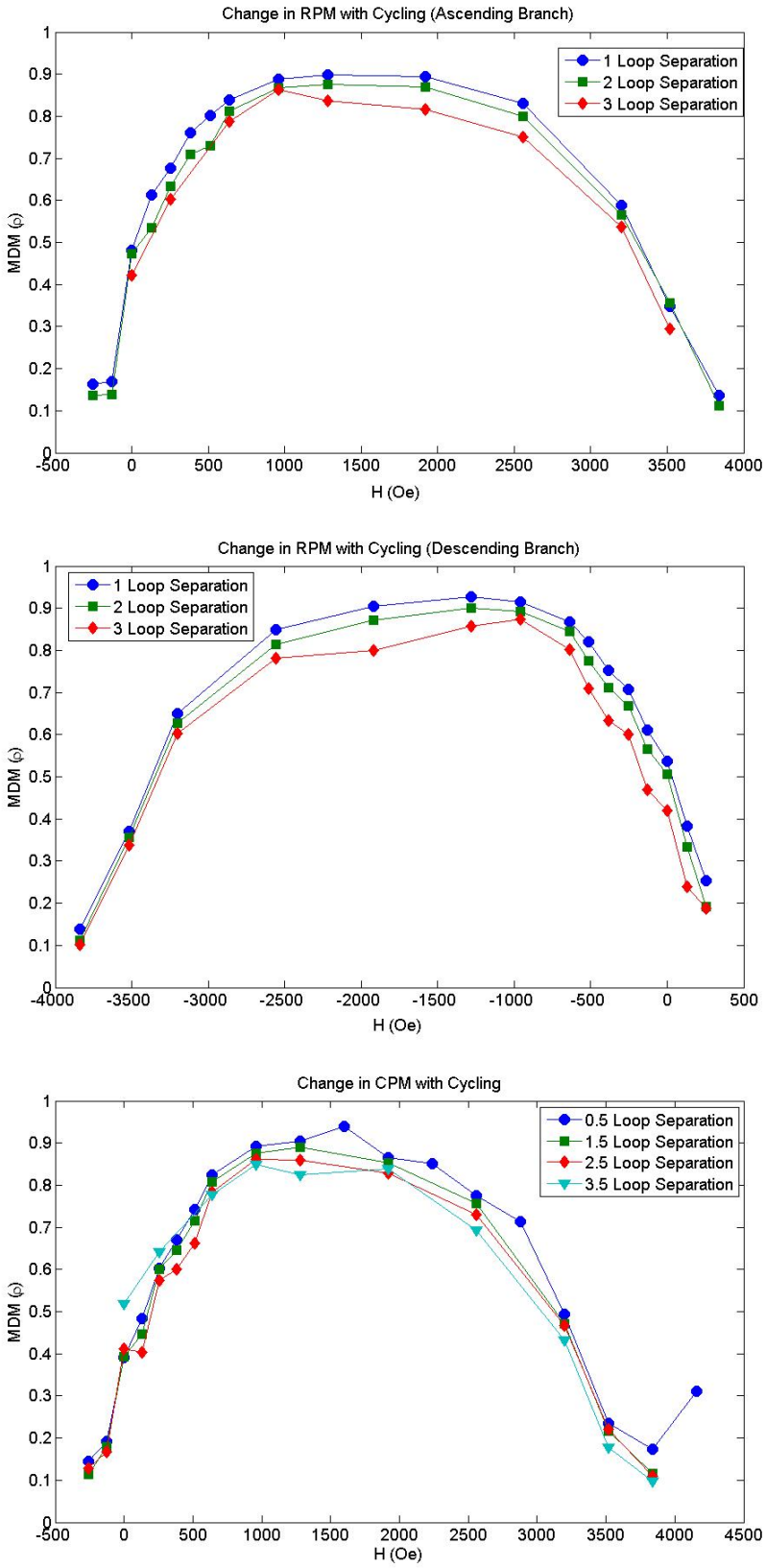

Figure 3.1 RPM and CPM graphs for the sample when it underwent Zero Field Cooling.

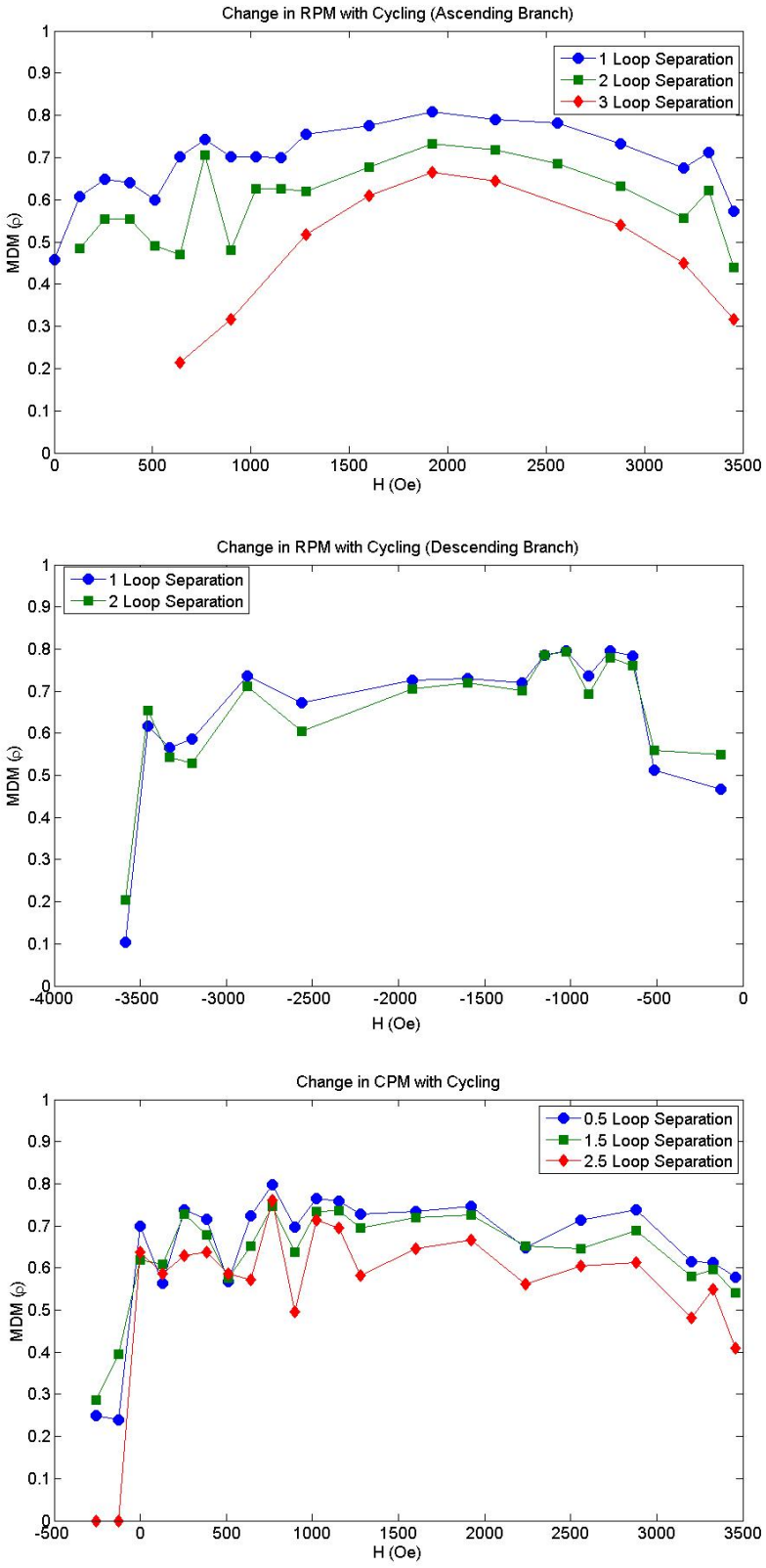

Figure 3.2 RPM and CPM graphs for the sample when it underwent field cooling with a field of 640 Oe.

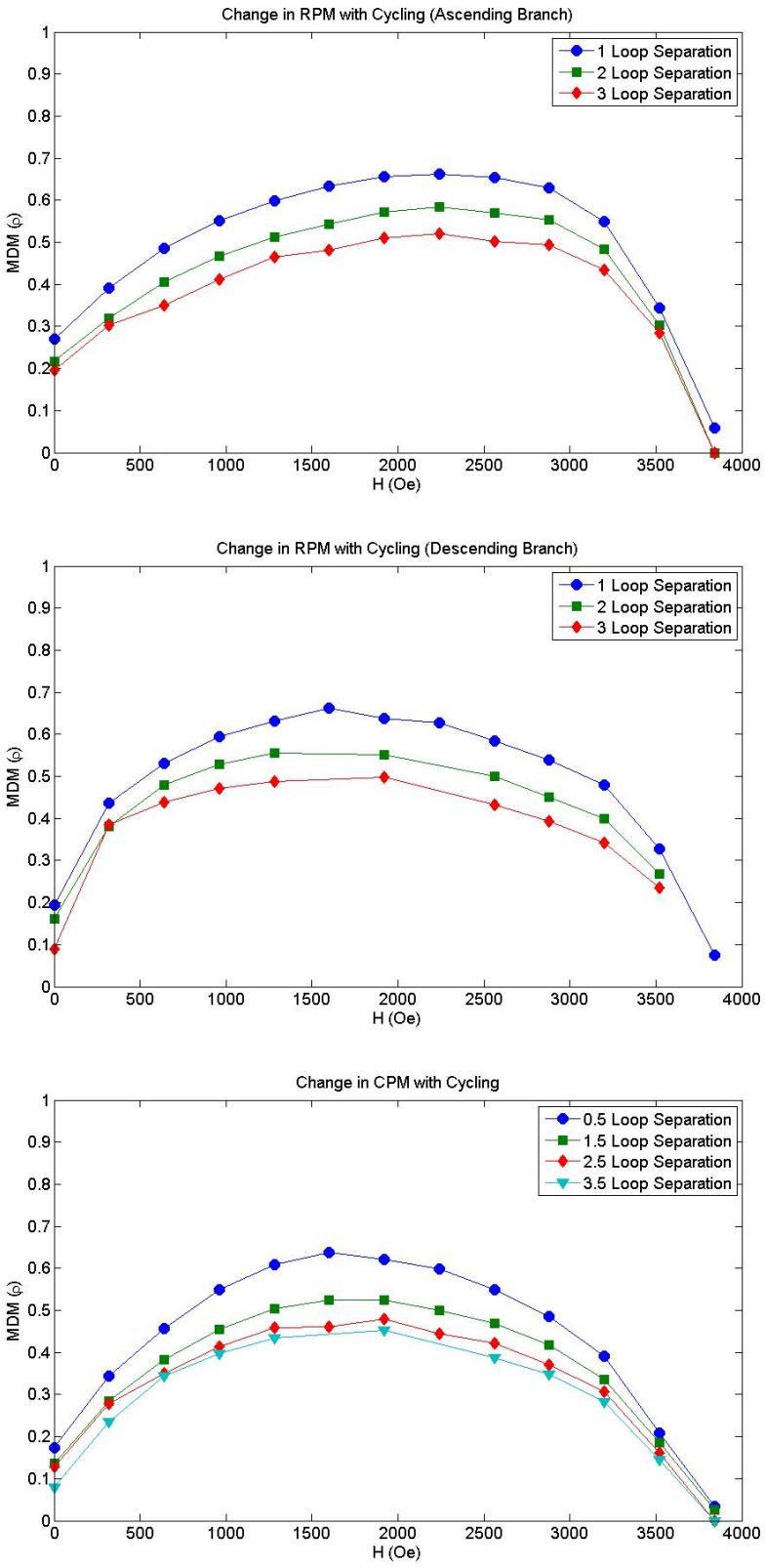

Figure 3.3 RPM and CPM graphs for the sample when it underwent field cooling with a field of 1280 Oe.

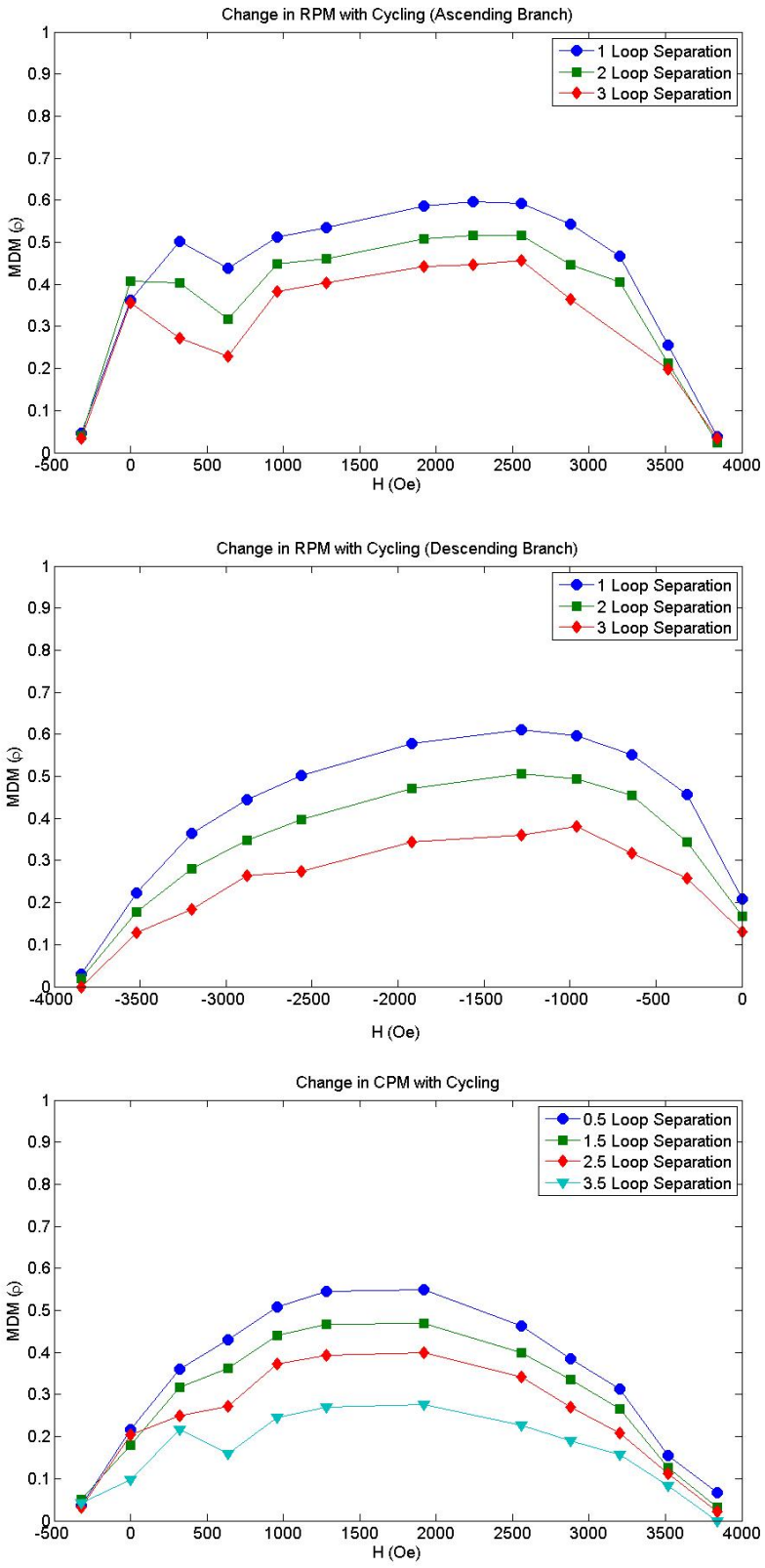

Figure 3.4 RPM and CPM graphs for the sample when it underwent field cooling with a field of 1920 Oe.

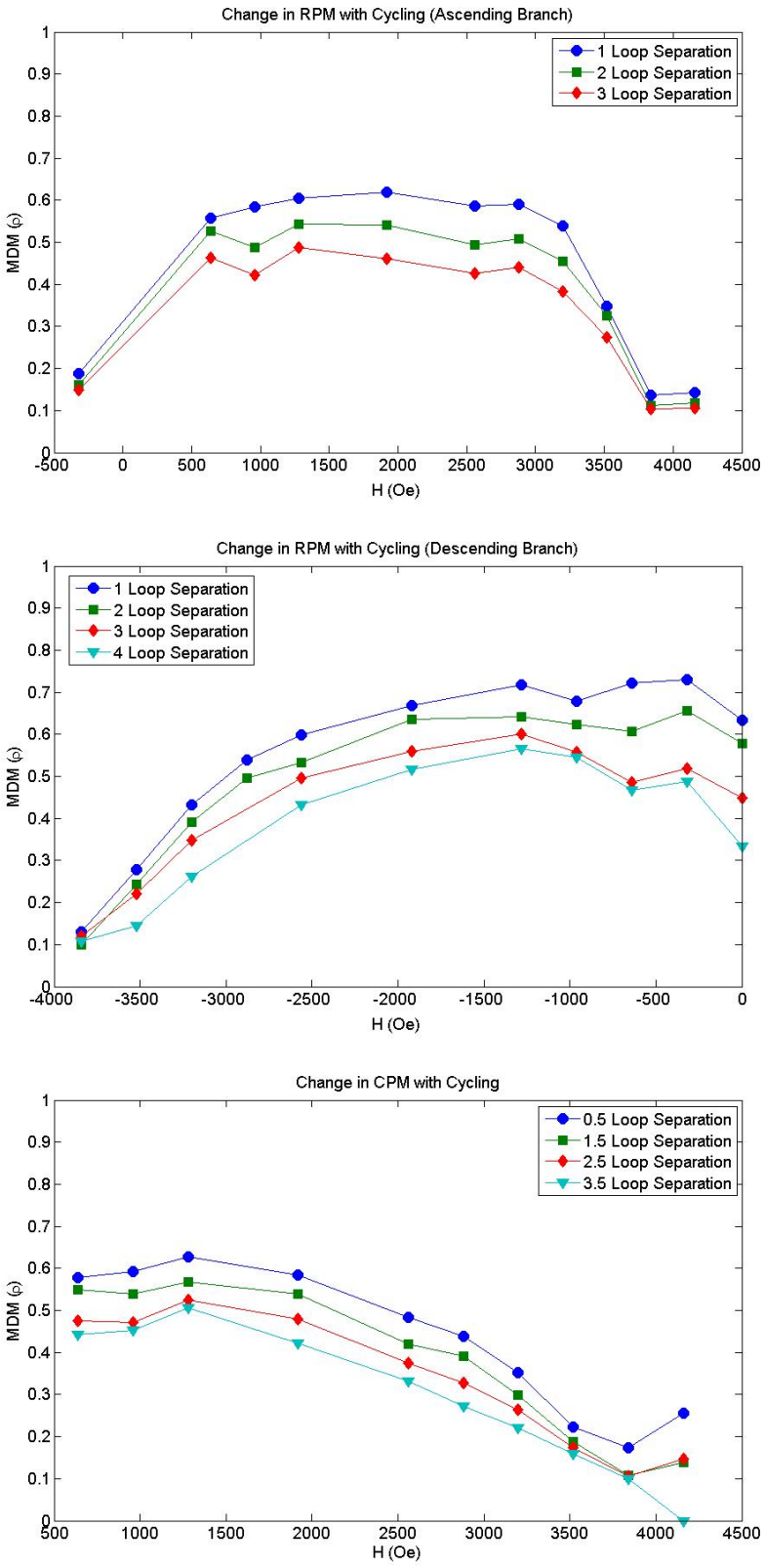

Figure 3.5 RPM and CPM graphs for the sample when it underwent field cooling with a field of 2240 Oe.

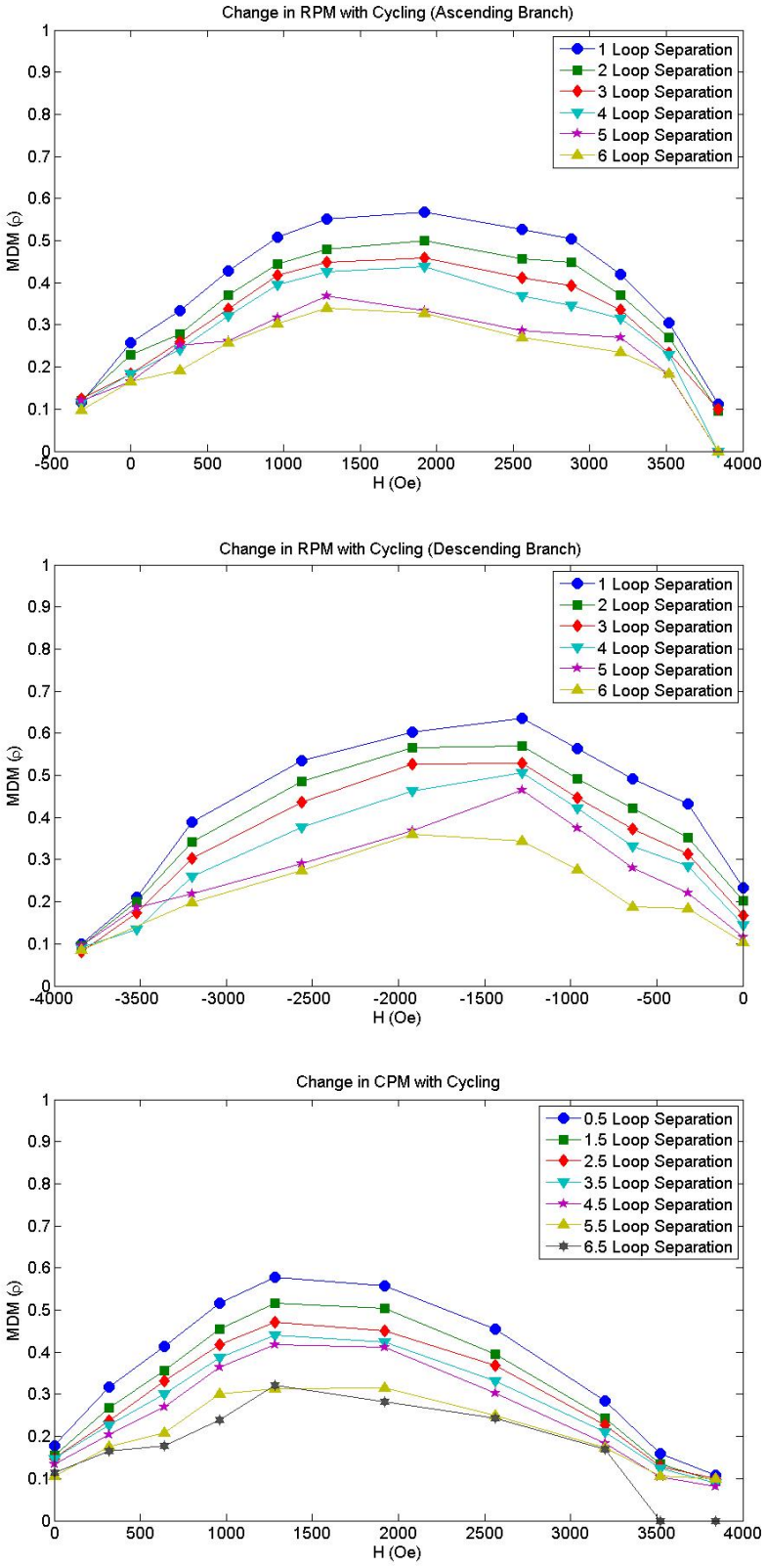

Figure 3.6 RPM and CPM graphs for the sample when it underwent field cooling with a field of 2560 Oe.

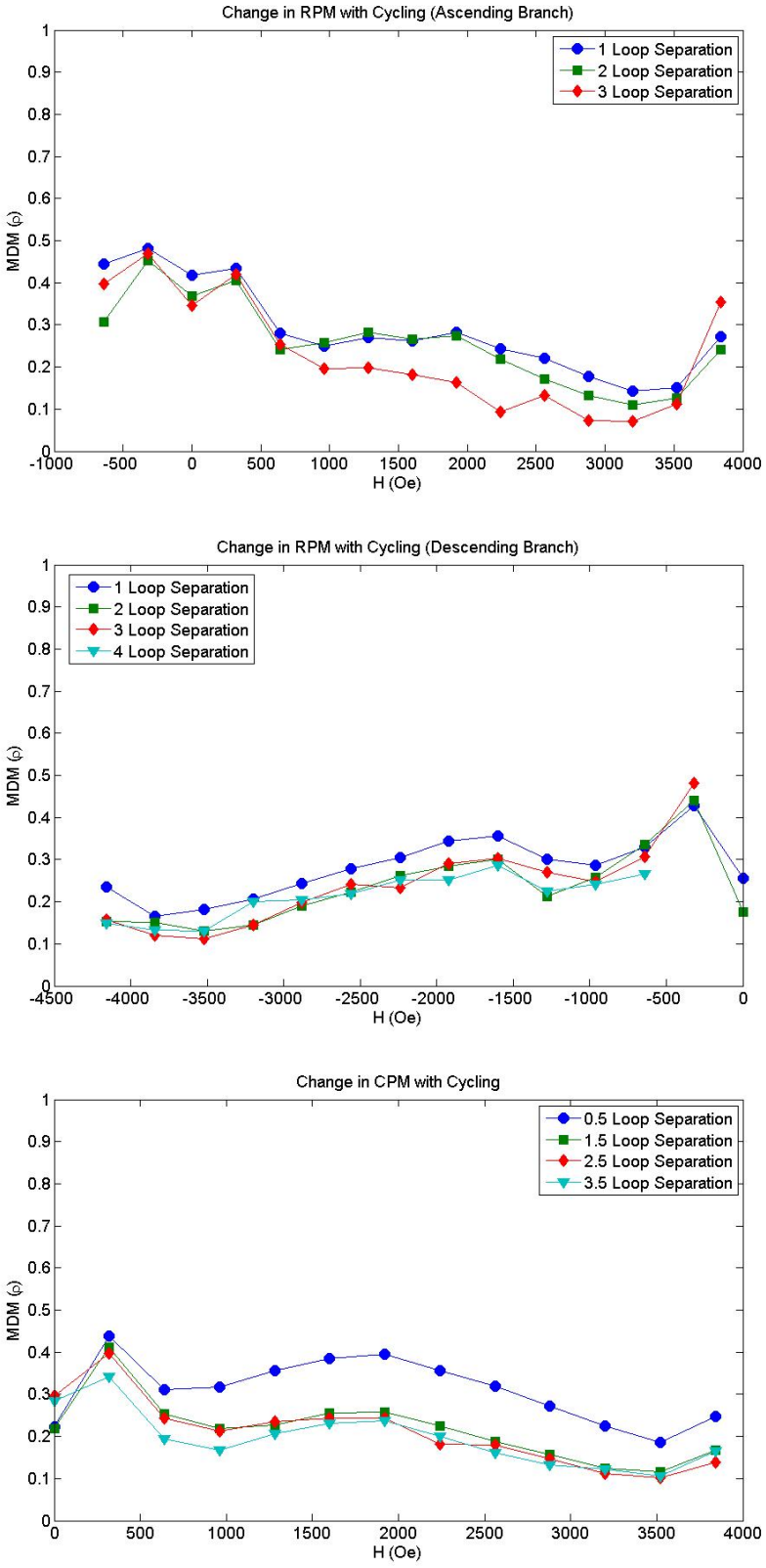

Figure 3.7 RPM and CPM graphs for the sample when it underwent field cooling with a field of 3200 Oe.

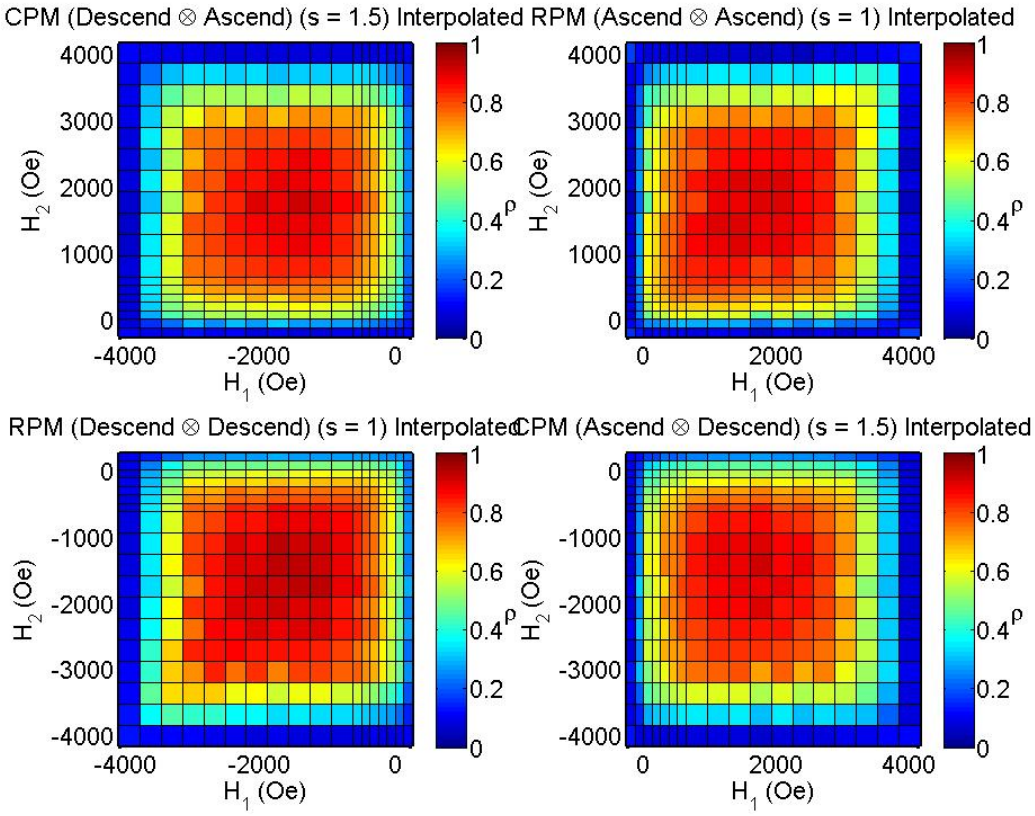

Figure 3.8 Interfield maps for the zero field cooling series.

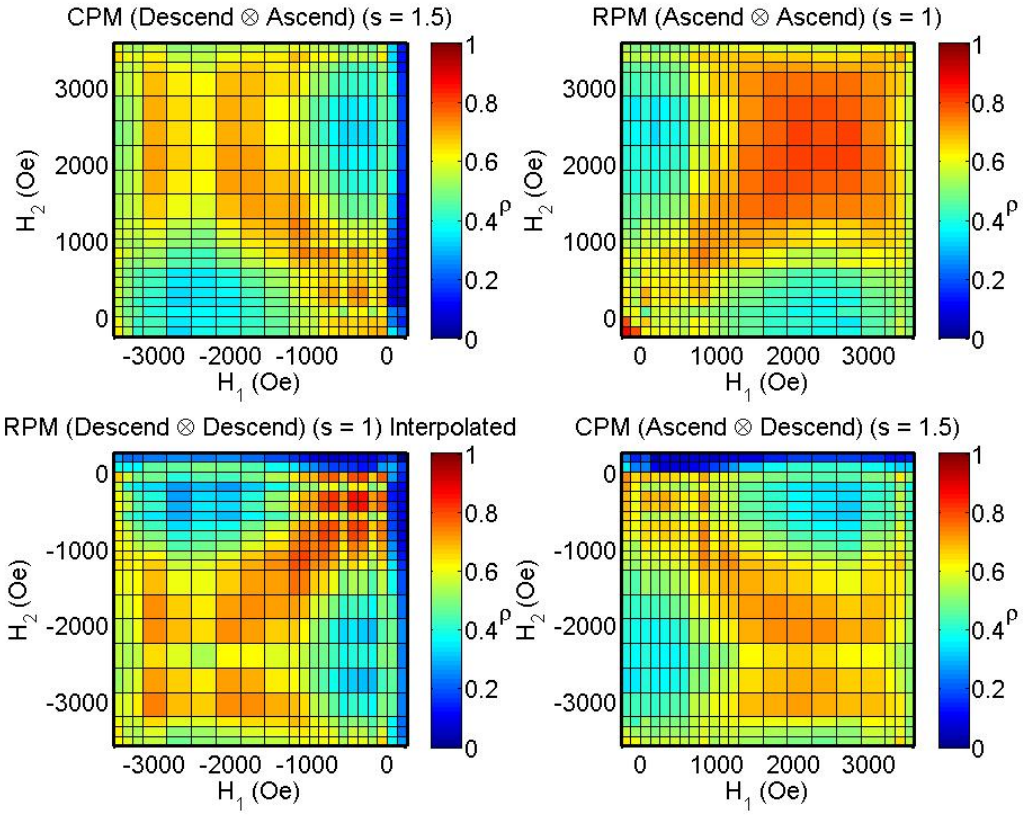

Figure 3.9 Interfield maps for the 640 Oe field cooling series.

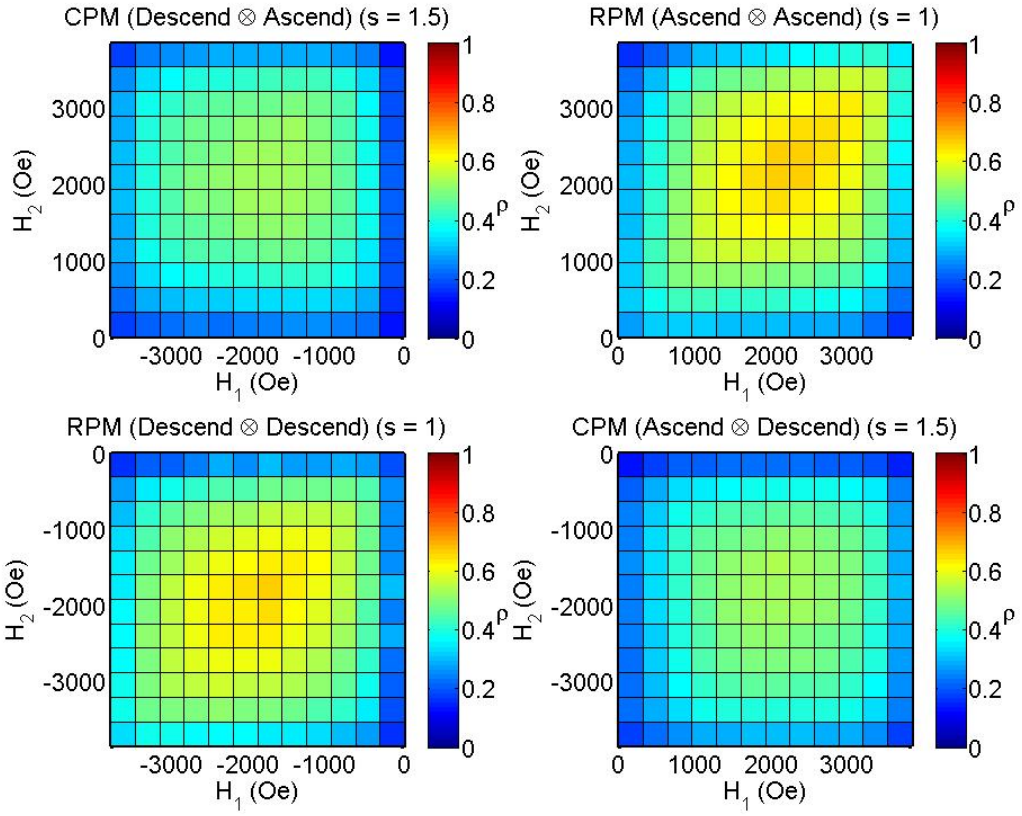

Figure 3.10 Interfield maps for the 1280 Oe field cooling series.

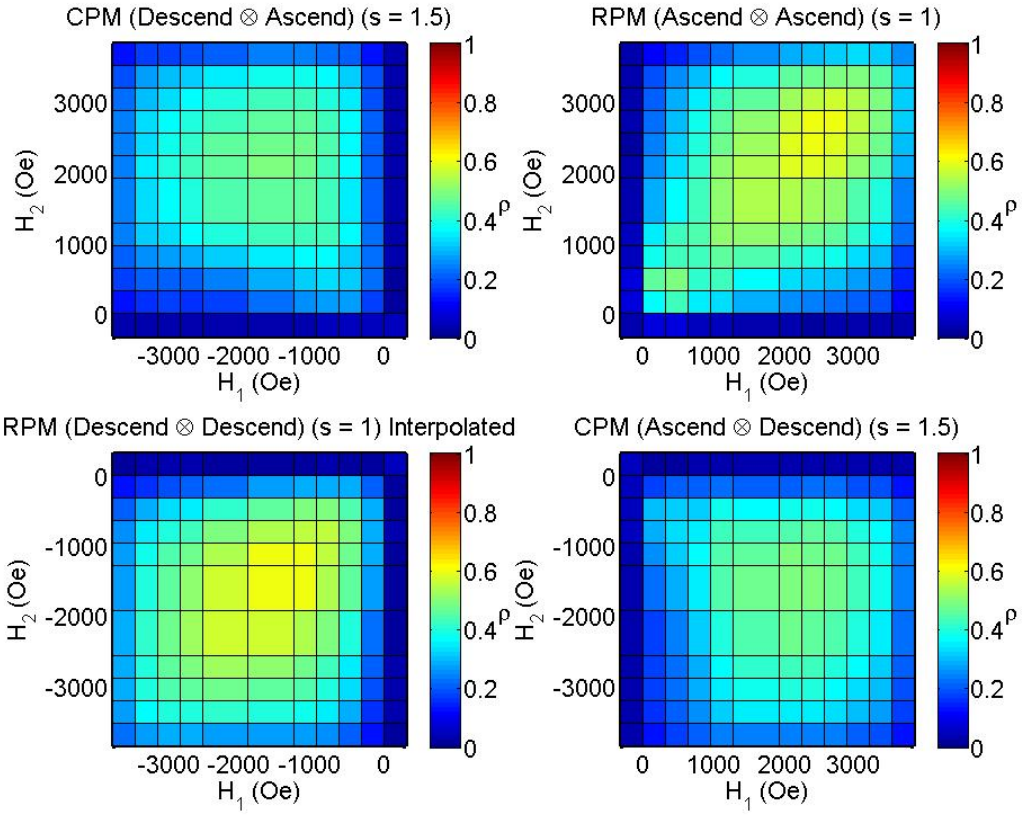

Figure 3.11 Interfield maps for the 1920 Oe field cooling series.

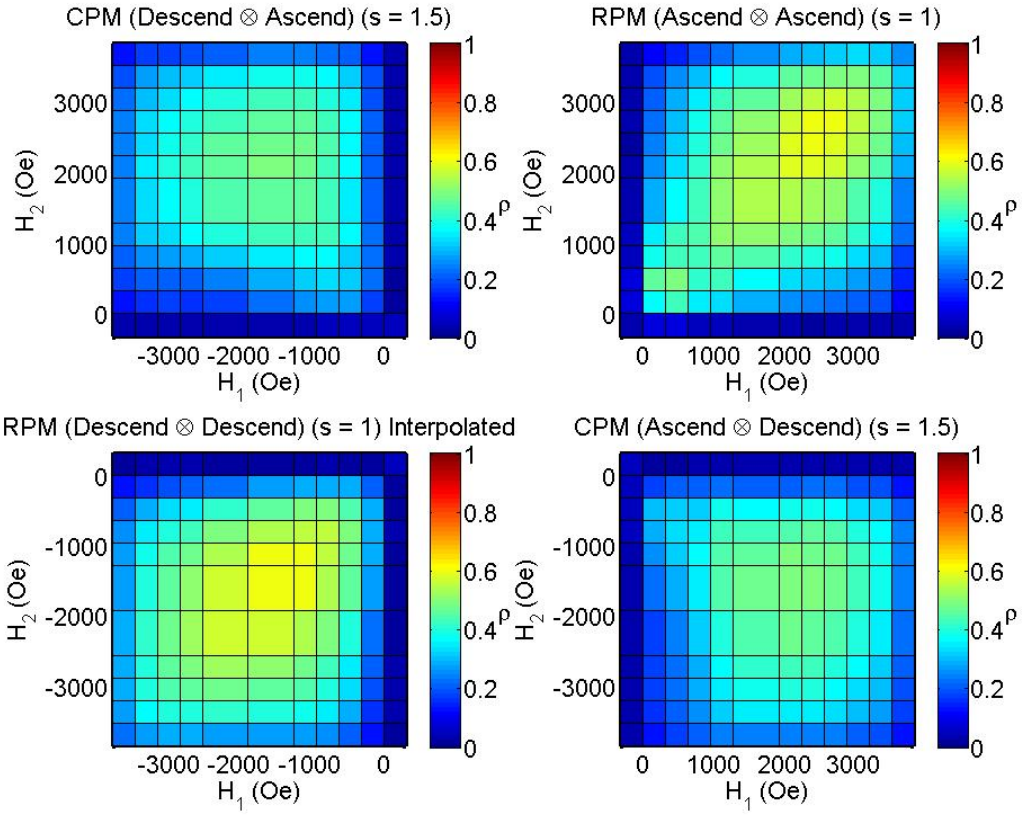

Figure 3.12 Interfield maps for the 1920 Oe field cooling series.

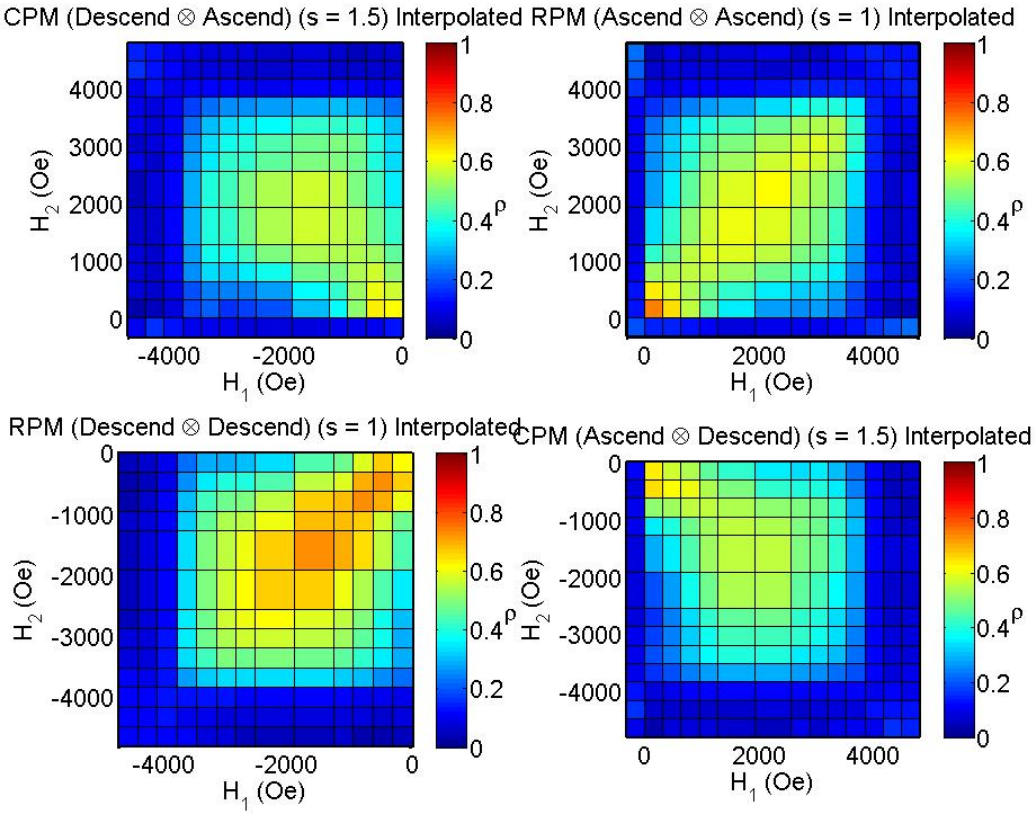

Figure 3.13 Interfield maps for the 2240 Oe field cooling series.

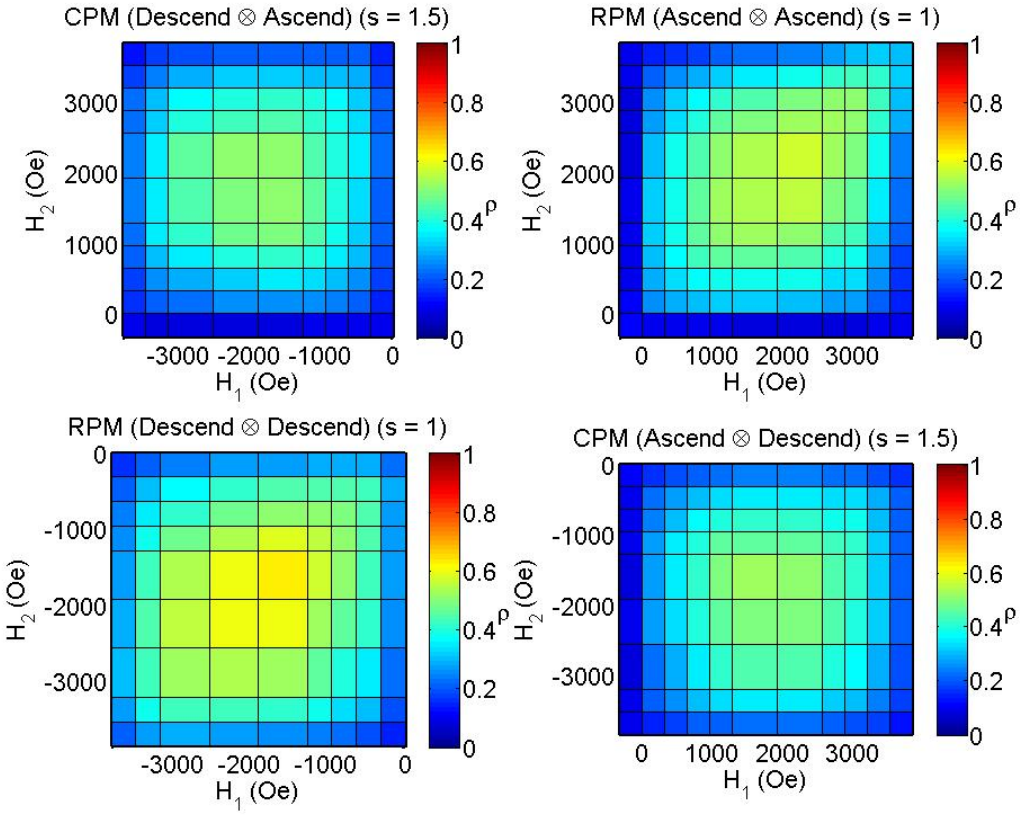

Figure 3.14 Interfield maps for the 2560 Oe field cooling series.

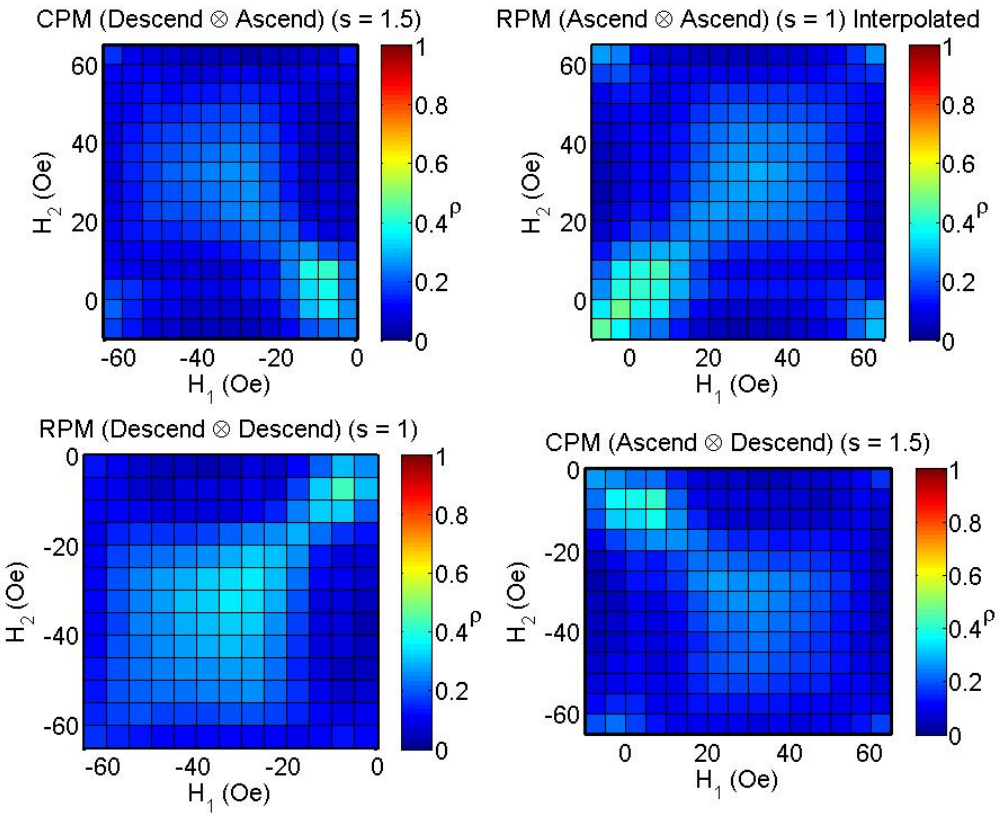

Figure 3.15 Interfield maps for the 3200 Oe field cooling series.

actually stays high on a plateau in the coercive region. This is where the net magnetization of the sample is near zero, i.e. there are approximately equal numbers of up and down domains. It also appears that with greater H_{FC}, the plateau tends to narrow - there is a smaller region of high MDM. More importantly, the region of highest MDM shifts with increasing H_{FC}. This is especially evident in Fig. 3.17 and 3.18. These effects are caused by the exchange coupling between the antiferromagnetic and ferromagnetic layers. The antiferromagnetic layer serves as a template which at low temperature stays magnetically 'frozen', i.e. it does not respond to the varying external field. Thus, due to exchange coupling the sample has a tendency to return to a domain morphology similar to the state it had when the antiferromagnetic spins were locked in place. With greater H_{FC}, the template is shifted to a different state.

Fig. 3.16 show what the antiferromagnetic template would look like during ZFC. In both images, the antiferromagnetic template is the lower layer. As the ferromagnetic layer propagates from nucleation in (a) to the coercive point (b), it follows the antiferromagnetic layer. However, in FC, the antiferromagnetic template would not have an equal number of up and down domains, but would instead be skewed in the direction of H_{FC}. Thus, in a state like $H_{FC} = 3200$ Oe, the template would actually look like the ferromagnetic layer in Fig. 3.16(a) where the template would essentially be one large domain with a few, small, anti-parallel domains interspersed.

3.3 Comparison Between Zero Field Cooling and Field Cooling States

When these results found in field cooling are compared to the ZFC results found previously, it is quickly apparent that there is lower memory in FC. When the sample underwent ZFC, it exhibited MDM of over 90%. [12] This high memory even persisted after several loops.

A field cooling state still shows high memory, but it decreases with increasing H_{FC}. This trend

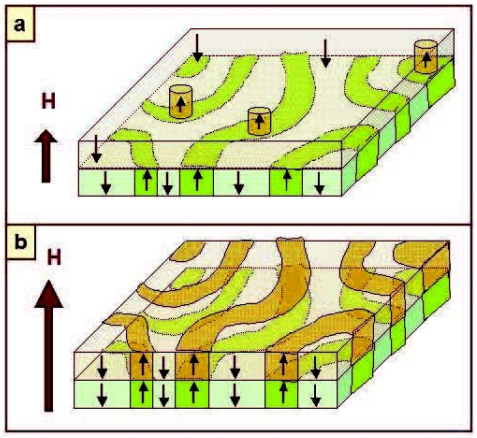

Figure 3.16 Sketch of magnetic domains nucleating (a) and propagating toward the coercive point (b). In both sketches, the ferromagnetic layer lays on top and the antiferromagnetic lays below. [4]

is initial fairly linear as shown in Fig. 3.19, but there is a dramatic decrease once the H_{FC} reaches a value close to saturation. It should be noted that this is the maximum MDM in the coercive region. The 3200 Oe series actually had higher memory outside of the coercive region. The stability in MDM over several loops is also weaker in the FC state. Here the memory between adjacent loops is significantly higher than memory between field cycles done further apart.

The fact that the MDM goes to only 30% or so with the greatest H_{FC} illustrates that MDM is indeed a consequence of exchange coupling. When that large of a field (3200 Oe or 0.32 T) is applied during cooling, the ferromagnetic domains are largely saturated, thus the antiferromagnetic layer's uncompensated spins are also saturated. This effectively removes the template the ferromagnetic domains were using to return to the same morphology and eliminates the MDM. Instead, at this highest FC state, there are only a few domains left in the template which instead induces some MDM toward nucleation.

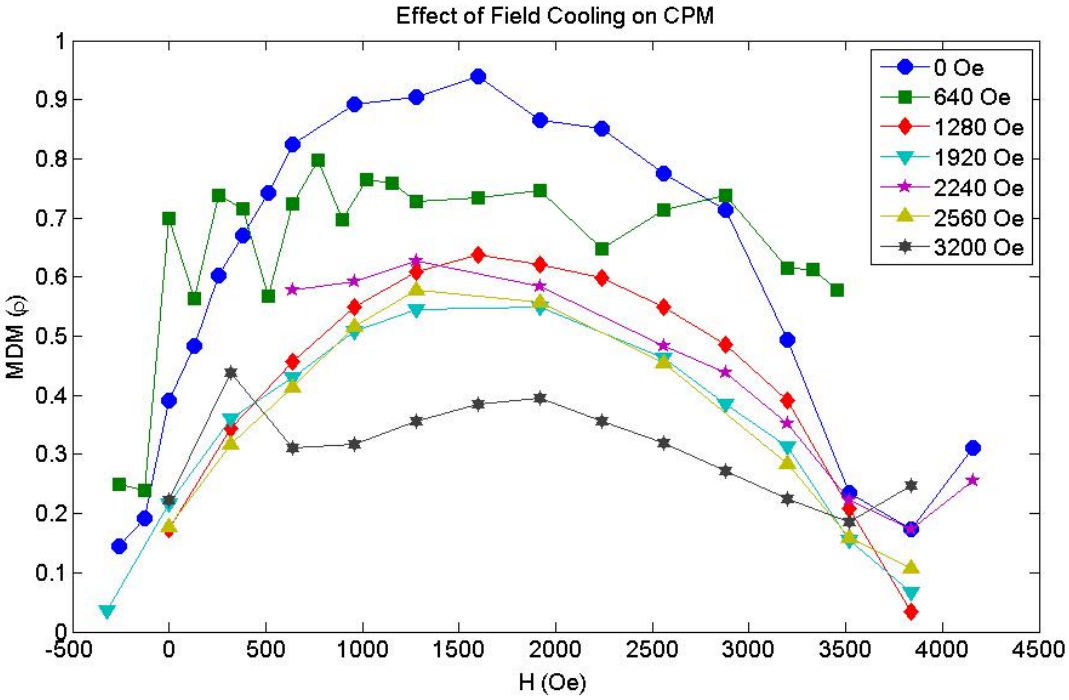

Figure 3.17 A comparison of CPM values for various H_{FC} series show the same decrease as the RPM comparison.

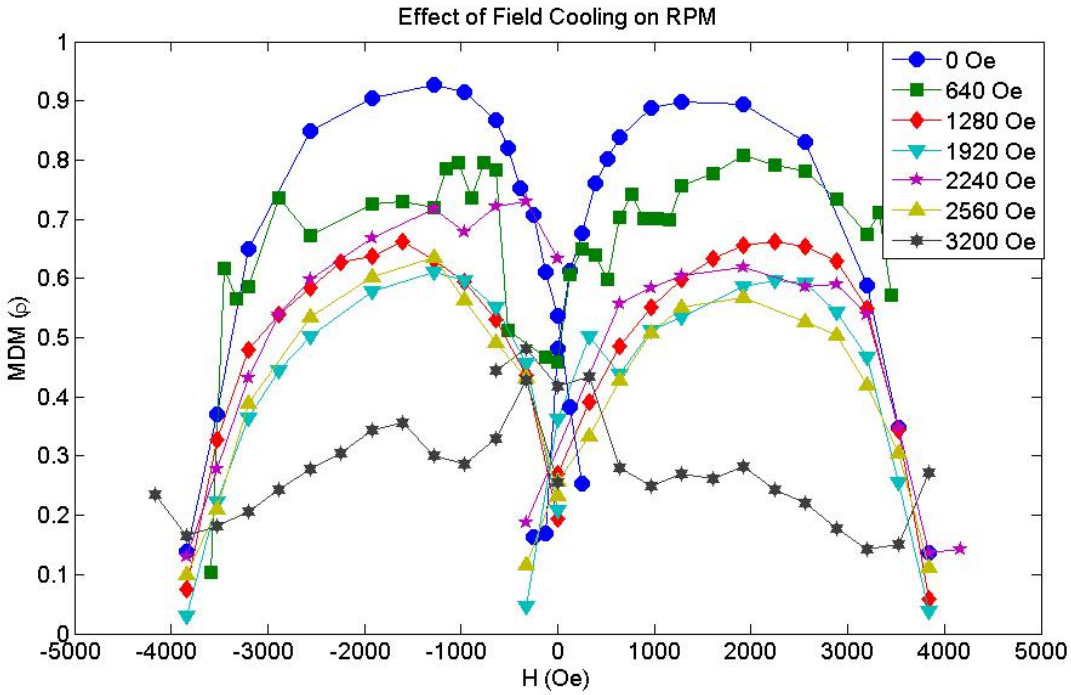

Figure 3.18 This graph shows that the greater the field applied during cooling (H_{FC}), the less memory there is. It also shows that there is a trend for the maximum ρ to occur at a greater field values in the loop. The curves also become less symmetrical. Finally, it is important to note that eventually the MDM effectively disappears.

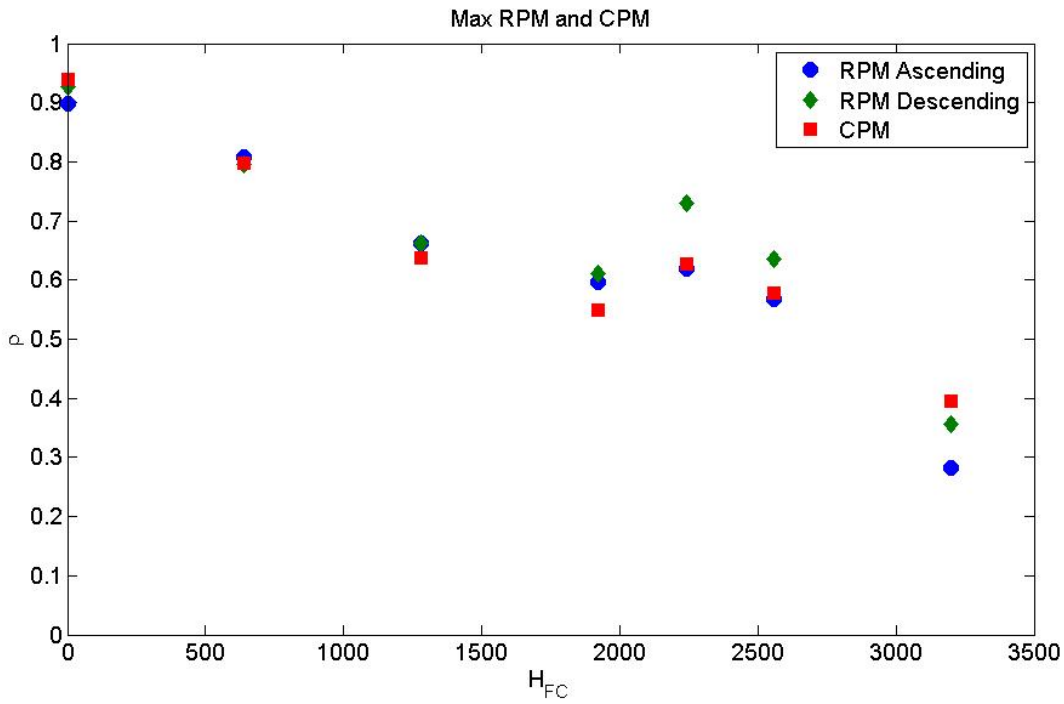

Figure 3.19 This graph shows the maximum RPM and CPM for a given cooling field. There is a fairly linear trend initially as the MDM decreases with greater H_{FC}, but there is a dramatic decrease between 2500 and 3200 Oe as this value leads to saturation of the sample.

3.4 Conclusions

Exchange coupling provides a good method for inducing high memory in the coercive region. This has been shown through both ZFC and field cooling measurements. Using antiferromagnetic materials and the induced exchange coupling provides a template for the ferromagnetic layer to exhibit high MDM in the coercive region where the net magnetization of the sample is near zero. It appears, however, that field cooling reduces the benefit of the exchange coupling and lowers the MDM of the material. The loss of memory is likely due to the change undergone by the antiferromagnetic template.

Looking back at Fig. 3.18, it is interesting to note that there is actually higher memory in the nucleation state than the coercive state when the sample underwent $H_{FC} = 3200$ Oe. This effect

may be due to the template consisting of mostly small domains in this state, as visualized in Fig. (the new 50 amp MFM). These small domains may in turn serve as nucleation sites similar to the effect caused by defects in the material. This is certainly an effect that warrants additional study.

3.5 Perspectives

These results are significant but preliminary. To further characterize the behavior of MDM, we will fill in missing FC values. There is a significant decrease in memory as the H_{FC} nears H_S and it would be instructive to have series taken at intermediate values in this region. We plan to do further experiments in which the step size in the applied field is smaller to produce a fuller range of data. We also have already begun to do some experiments at the APS at higher temperatures and will continue to explore the effect of temperature. It would be interesting to explore the effect of film thickness on memory. We have performed some analysis on the effect of Co thickness on the shape of the hysteresis loop with Co/Pt multilayers. It would be interesting to see if there is a similar effect on the hysteresis loop of our sample with a change in Co thickness and to see if this has an effect on MDM. Finally, we would like to expand this research into other types of magnetic material other than cobalt. This area of research offers to greatly improve magnetic data storage as a viable long-term option; we want to add to the fundamental knowledge of these materials so that the best choices can be made.

Bibliography

[1] S. Hashimoto, Y. Ochiai, and K. Aso, "Perpendicular magnetic anisotropy and magnetostriction of sputtered Co/Pd and Co/Pt multilayered films," Journal of Applied Physics **66,** 4909–4916 (1989).

[2] H. Richter, "Density limits imposed by the microstructure of magnetic recording media," Journal of Magnetism and Magnetic Materials **321,** 467–476 (2009).

[3] M. S. Pierce, "Disorder-induced magnetic memory: Experiments and theories," Physical Review B 75 (2007).

[4] K. Chesnel, E. E. Fullerton, M. J. Carey, J. B. Kortright, and S. D. Kevan, "Magnetic memory in ferromagnetic thin films via exchange coupling," Physical Review B 78 (2008).

[5] B. Wilcken, "Magnetic Memory in Exchange-Bias Thin Films," BYU - Senior Thesis (2009).

[6] J. Nelson, "Spatial and Temperature Dependance of Magnetic Domain Memory Induced by Exchange-Coupling," BYU - Senior Thesis (2010).

[7] J. Kortright, D. Awschalom, J. Stohr, S. Bader, Y. Idzerda, S. Parkin, I. Schuller, and H. Siegmann, "Research frontiers in magnetic materials at soft X-ray synchrotron radiation facilities," Journal of Magnetism and Magnetic Materials **207,** 7–44 (1999).

[8] Blume, Journal of Applied Physics **57,** 3615 (1985).

[9] J. P. Hannon and et al., Physical Review Letters **61,** 1245 (1988).

[10] C. for X-Ray Optics and A. L. Source, *X-Ray Data Booklet* (Lawrence Berkeley National Lab, University of California, January 2009).

[11] K. Chesnel, J. J. Turner, M. Pfeifer, and S. D. Kevan, "Probing complex materials with coherent soft X-rays," Applied Physics A-Materials Science and Processing **92,** 431 (2008).

[12] K. Chesnel, J. Nelson, B. Wilcken, and S. D. Kevan, "Mapping spatial and field dependence of magnetic domain memory by soft X-ray speckle metrology," Journal of Synchrotron Radiation **19,** 293–306 (2012).